

Communication

# Zn(II) Metal–Organic Frameworks with a Long Spacer Ligand and a Tricarboxylate Coligand

Dong Hee Lee  and In-Hyeok Park \* 

Graduate School of Analytical Science and Technology (GRAST), Chungnam National University, Daejeon 34134, Republic of Korea

\* Correspondence: ipark@cnu.ac.kr

**Abstract:** The preparations and structural characteristics of three-dimensional Zn(II) metal-organic frameworks (MOFs) with dipyrindyl-olefin and tricarboxylate are reported. The solvothermal reactions of zinc(II) nitrate hexahydrate, 1,4-bis [2-(4-pyridyl)ethenyl]benzene (bpeb), and 4,4',4''-benzene-1,3,5-triyl-tris(benzoic acid) (H<sub>3</sub>btb) furnished three Zn(II) MOFs (1–3) with new topologies. Depending on the temperature or mole-ratio variations, self-interpenetrated [Zn<sub>2</sub>(bpeb)(btb)(OH)]·DMF·H<sub>2</sub>O (1), noninterpenetrated [Zn<sub>3</sub>(btb)<sub>2</sub>(bpeb)]·xSolvent (2), and fourfold interpenetrated [Zn<sub>2</sub>(Hbtb)<sub>2</sub>(bpeb)] [Zn<sub>2</sub>(Hbtb)<sub>2</sub>(bpeb)] [Zn<sub>4</sub>(Hbtb)<sub>4</sub>(bpeb)<sub>2</sub>] (3) structures were generated with different molecular building blocks. It is interesting that although all three MOFs contain the same metal cation, anion, and spacer ligand, they show different emissions due to structure and connectivity.

**Keywords:** MOFs; zinc; tricarboxylate; coligand; mole-ratio; long spacer ligand



**Citation:** Lee, D.H.; Park, I.-H. Zn(II) Metal–Organic Frameworks with a Long Spacer Ligand and a Tricarboxylate Coligand. *Crystals* **2023**, *13*, 1266. <https://doi.org/10.3390/cryst13081266>

Academic Editors: Helmut Cölfen, Sławomir Grabowski, Heike Lorenz, Jesús Sanmartín-Matalobos and Shujun Zhang

Received: 16 July 2023

Revised: 12 August 2023

Accepted: 14 August 2023

Published: 17 August 2023



**Copyright:** © 2023 by the authors. Licensee MDPI, Basel, Switzerland. This article is an open access article distributed under the terms and conditions of the Creative Commons Attribution (CC BY) license (<https://creativecommons.org/licenses/by/4.0/>).

## 1. Introduction

The crystal engineering of coordination polymers (CPs) and metal–organic frameworks (MOFs) has advanced significantly, with a matured design component [1–7]. Currently, the focus has shifted towards exploration and understanding the relationships between structure, function, and properties [8,9]. In essence, selecting suitable metal cations and spacer ligands allows for control over the interpenetration, cavities, channels, topology, connectivity, and proximity of reactive functional groups within the lattice of coordination networks. Nonetheless, throughout the crystallization process, the prevailing influence of connectivity and topology remains attributable to kinetic factors. Crystals tend to maximize packing density, leading to voids being occupied by guests, uncoordinated ligands, or counterions, and sometimes resulting in interpenetration [4,10,11]. As the length of linear spacers is extended, it is observed that three-dimensional (3D) coordination polymers have a tendency to display interpenetration, and longer spacer ligands generally enhance the degree of interpenetration in structures that are already interpenetrated [12–18].

Furthermore, interpenetration is a common phenomenon in MOFs and CPs, with significant implications for pore engineering and various properties like gas separation, gas sensing, catalysis, drug delivery, energy storage, electric devices, thermal insulation, etc. [18–29]. The degree of interpenetration can be altered experimentally through factors such as reaction temperature, reactant ratio, solvent concentration, and solvent nature. For example, under conditions of elevated temperature and concentration, a pillared-layer structure with twofold interpenetration is favored, whereas reduced temperature and concentration lead to the formation of its noninterpenetrated counterpart [15]. The use of different amide-based solvents in solvothermal synthetic conditions can vary the interpenetration from three- to fivefold in diamondoid MOFs, where the interpenetration level affects their gas uptake properties [30]. Various methods, such as liquid-phase epitaxial growth and sonochemical techniques, offer control over interpenetration and catenation [31,32]. How gas sorption properties, chirality, nonlinear optical properties, and the sensing of

specific substances like ammonia and nitrobenzene are influenced by the degree of interpenetration has been explored [21–23,33–39].

Herein, we report the preparations of three MOFs from zinc(II) salt, 4,4',4''-benzene-1,3,5-triyl-tris(benzoic acid) (H<sub>3</sub>btb), and 1,4-bis[2-(4-pyridyl)ethenyl]benzene (bpeb), showing various interpenetration modes and new topologies (Figure 1 and Table 1). Several MOFs with various molecular building blocks via the self-assembly of the long spacer ligand, bpeb, and various Zn(II)-carboxylates have been reported [40–43]. In this study, it was possible to synthesize MOFs with new topologies by employing the large molecule btb tricarboxylate. These three structures (1–3) were constructed from different repeating units under different experimental conditions. The self-interpenetrated structure (1), noninterpenetrated rotaxane structure in a tricarboxylate plane threaded by bpeb (2), and four-interpenetrated three-dimensional (3D) network structure (3) are interesting and advance our structural knowledge in molecular machines like rotaxanes.

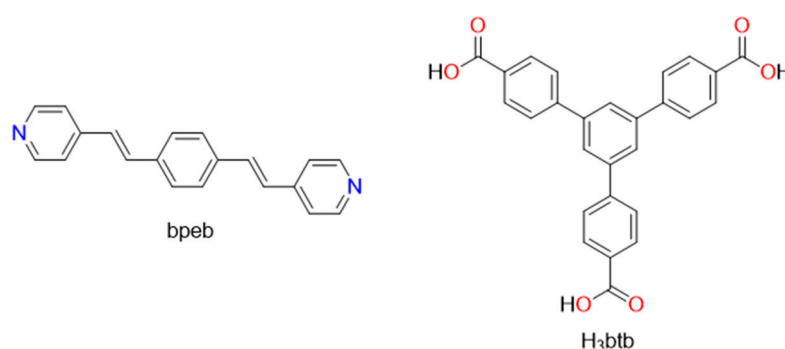


**Figure 1.** The bpeb and H<sub>3</sub>btb ligands used in this work.

**Table 1.** Crystal and experimental data and refinement parameters.

	1	2	3
Formula	C <sub>47</sub> H <sub>31</sub> N <sub>2</sub> O <sub>7</sub> Zn <sub>2</sub>	C <sub>74</sub> H <sub>46</sub> N <sub>2</sub> O <sub>12</sub> Zn <sub>3</sub>	C <sub>296</sub> H <sub>184</sub> N <sub>8</sub> O <sub>48</sub> Zn <sub>8</sub>
Formula weight	866.48	1351.24	5143.46
Temperature (K)	173	173	173
Crystal system	Orthorhombic	Monoclinic	Monoclinic
Space group	<i>Fdd2</i>	<i>C2/c</i>	<i>P2<sub>1</sub>/c</i>
<i>Z</i>	16	4	2
<i>a</i> (Å)	60.5386(9)	11.4402(4)	16.3093(12)
<i>b</i> (Å)	62.2276(10)	30.8405(10)	27.4589(19)
<i>c</i> (Å)	5.90860(10)	27.0931(9)	48.052(3)
<i>α</i> (°)	90	90	90
<i>β</i> (°)	90	96.884(2)	97.288(4)
<i>γ</i> (°)	90	90	90
<i>V</i> (Å <sup>3</sup> )	22,258.7(6)	9490.1(6)	21,346(3)
<i>D</i> <sub>calc</sub> (g/cm <sup>3</sup> )	1.034	0.946	0.800
2θ <sub>max</sub> (°)	52.00	52.00	52.00
<i>R</i> <sub>1</sub> , <i>wR</i> <sub>2</sub> [ <i>I</i> > 2σ( <i>I</i> )]	0.0866, 0.2656	0.0620, 0.1673	0.0836, 0.1800
<i>R</i> <sub>1</sub> , <i>wR</i> <sub>2</sub> [all data]	0.0980, 0.2826	0.1161, 0.1845	0.1939, 0.2066
Goodness-of-fit on <i>F</i> <sup>2</sup>	1.010	0.994	0.819
No. of reflection used [ <i>I</i> > 2σ( <i>I</i> )]	10834 [ <i>R</i> <sub>int</sub> = 0.0513]	9302 [ <i>R</i> <sub>int</sub> = 0.1134]	41682 [ <i>R</i> <sub>int</sub> = 0.1771]
Refinement	55166	77799	62360
Largest diff. peak and hole	1.956 and −1.655 e·Å <sup>−3</sup>	0.406 and −0.431 e·Å <sup>−3</sup>	1.153 and −1.232 e·Å <sup>−3</sup>

## 2. Materials and Methods

### 2.1. General Procedures

All chemicals were purchased from commercial sources and used as received. All solvents used were of reagent grade. The bpeb ligand was synthesized via the reported

procedure [44]. Elemental analyses were carried out on a LECO CHNS-932 elemental analyzer. The solid-state emission spectra were obtained from a Perkin Elmer LS 55 luminescence spectrometer. The FT-IR spectra were recorded using a Varian 640-IR FT-IR Spectrometer with KBr pellets. The thermogravimetric curves were collected in a TA Instruments TGA-Q50 thermogravimetric analyzer. The samples were heated at a constant rate of  $10\text{ }^{\circ}\text{C min}^{-1}$  from room temperature to  $700\text{ }^{\circ}\text{C}$  in a continuous-flow nitrogen atmosphere. The powder X-ray diffraction (PXRD) patterns were recorded on a Siemens D500 diffractometer with graphite monochromatized Cu-K $\alpha$  radiation ( $\lambda = 1.54056\text{ \AA}$ ) at room temperature ( $23\text{ }^{\circ}\text{C}$ ). The single-crystal X-ray data were collected at the Korea Basic Science Institute (KBSI, Western Seoul Center, South Korea).

### 2.2. Preparation of $[\text{Zn}_2(\text{bpeb})(\text{btb})(\text{OH})]\cdot\text{DMF}\cdot\text{H}_2\text{O}$ (1)

A mixture of bpeb (20.1 mg, 0.070 mmol),  $\text{H}_3\text{btb}$  (30.8 mg, 0.070 mmol), and  $\text{Zn}(\text{NO}_3)_2\cdot 4\text{H}_2\text{O}$  (18.4 mg, 0.070 mmol) in DMF (3 mL),  $\text{H}_2\text{O}$  (1 mL), and DMSO (0.5 mL) was placed in a 5 mL glass tube, and then 2–3 drops of 0.1 M NaOH solution was added. The tube was sealed and kept at  $110\text{ }^{\circ}\text{C}$  for 48 h, followed by cooling to room temperature over 8 h. Green block-shaped crystals 1 suitable for X-ray analysis were obtained. IR (KBr pellet,  $\text{cm}^{-1}$ ): 3446, 3037, 2817, 1634, 1611, 1548, 1377, 1104, 1018, 853, 817, 770, 704, 672. Anal. Calcd for  $[\text{C}_{50}\text{H}_{41}\text{N}_3\text{O}_9\text{Zn}_2]$ : C, 62.64; H, 4.31; N, 4.38. Found: C, 62.79; H, 4.34; N, 4.40%.

### 2.3. Preparation of $[\text{Zn}_3(\text{btb})_2(\text{bpeb})]\cdot x\text{Solvent}$ (2)

A mixture of bpeb (20.1 mg, 0.070 mmol),  $\text{H}_3\text{btb}$  (15.4 mg, 0.035 mmol), and  $\text{Zn}(\text{NO}_3)_2\cdot 4\text{H}_2\text{O}$  (18.4 mg, 0.070 mmol) in DMF (3 mL),  $\text{H}_2\text{O}$  (1 mL), and DMSO (0.5 mL) was placed in a 5 mL glass tube, and then 2–3 drops of 0.1 M NaOH solution was added. The tube was sealed and kept at  $120\text{ }^{\circ}\text{C}$  for 48 h, followed by cooling to room temperature over 8 h. Green plate-shaped crystals 2 suitable for X-ray analysis were obtained. IR (KBr pellet,  $\text{cm}^{-1}$ ): 3021, 2806, 1638, 1629, 1537, 1369, 1121, 1017, 854, 812, 776, 701, 670. Anal. Calcd for  $[\text{C}_{80}\text{H}_{64}\text{N}_4\text{O}_{16}\text{Zn}_3]$  as  $[\text{Zn}_3(\text{btb})_2(\text{bpeb})]\cdot 2\text{DMF}\cdot 2\text{H}_2\text{O}$ : C, 62.66; H, 4.21; N, 3.65. Found: C, 63.01; H, 4.14; N, 3.49%.

### 2.4. $[\text{Zn}_2(\text{Hbtb})_2(\text{bpeb})][\text{Zn}_2(\text{Hbtb})_2(\text{bpeb})][\text{Zn}_4(\text{Hbtb})_4(\text{bpeb})_2]\cdot x\text{Solvent}$ (3)

A mixture of bpeb (20.1 mg, 0.070 mmol),  $\text{H}_3\text{btb}$  (31.1 mg, 0.071 mmol), and  $\text{Zn}(\text{NO}_3)_2\cdot 4\text{H}_2\text{O}$  (18.4 mg, 0.070 mmol) in DMF (3 mL),  $\text{H}_2\text{O}$  (1 mL), and DMSO (0.5 mL) was placed in a 5 mL glass tube, and then 2–3 drops of 0.1 M NaOH solution was added. The tube was sealed and kept at  $120\text{ }^{\circ}\text{C}$  for 48 h, followed by cooling to room temperature over 8 h. Green plate-shaped crystals 3 suitable for X-ray analysis were obtained. IR (KBr pellet,  $\text{cm}^{-1}$ ): 3023, 2821, 1641, 1609, 1523, 1362, 1101, 1025, 853, 817, 769, 708, 676. Anal. Calcd for  $[\text{C}_{305}\text{H}_{221}\text{N}_{11}\text{O}_{55}\text{Zn}_8]$  as  $[\text{Zn}_2(\text{Hbtb})_2(\text{bpeb})][\text{Zn}_2(\text{Hbtb})_2(\text{bpeb})][\text{Zn}_4(\text{Hbtb})_4(\text{bpeb})_2]\cdot 3\text{DMF}\cdot 4\text{H}_2\text{O}$ : C, 67.30; H, 4.09; N, 2.83. Found: C, 67.41; H, 4.15; N, 2.97%.

### 2.5. X-ray Crystallographic Analysis

The crystal structures of the crystallized samples of 1–3 were determined by single-crystal diffraction methods at the Korea Basic Science Institute (KBSI, Western Seoul Center, Daejeon, Korea). All crystals were picked up with paratone oil and mounted on a Bruker D8 Venture PHOTON III M14 diffractometer equipped with a graphite monochromated Mo K $\alpha$  ( $\lambda = 0.71073\text{ \AA}$ ) radiation source and a nitrogen cold stream ( $-100\text{ }^{\circ}\text{C}$ ). Data collection and integration were performed with SMART APEX3 (Bruker, Billerica, MA, USA, 2016) and SAINT (Bruker, 2016) [45,46]. The absorption correction was performed by a multiscan method implemented in SADABS [45]. The structure was solved by direct methods and refined by full-matrix least-squares on  $F^2$  using SHELXTL [47].

In all cases, all nonhydrogen atoms were refined anisotropically, and all hydrogen atoms were placed in idealized positions and refined isotropically in a riding manner along with their respective parent atoms. Due to the serious disorders of the lattice solvents,

MOFs 1–3 were squeezed by PLATON [48]. Relevant crystal data collection and refinement data for the crystal structures are summarized in Table S1.

CCDC 2278602–2278604 contains the supplementary crystallographic data for this paper. These data can be obtained free of charge via <http://www.ccdc.cam.ac.uk/conts/retrieving.html> (accessed on 8 July 2023) (or from the CCDC, 12 Union Road, Cambridge CB2 1EZ, UK; fax: +44-1223-336033; e-mail: deposit@ccdc.cam.ac.uk).

### 3. Results and Discussion

#### 3.1. Syntheses of CPs 1–3

Three three-dimensional MOFs (designated as 1–3) were prepared through solvothermal reactions involving  $\text{Zn}(\text{NO}_3)_2 \cdot 4\text{H}_2\text{O}$ , bpeb, and  $\text{H}_3\text{btb}$ . Despite utilizing the same solvent conditions, variations existed in the equimolar ratio and/or temperature applied during each reaction. The details are shown in Figure 2.

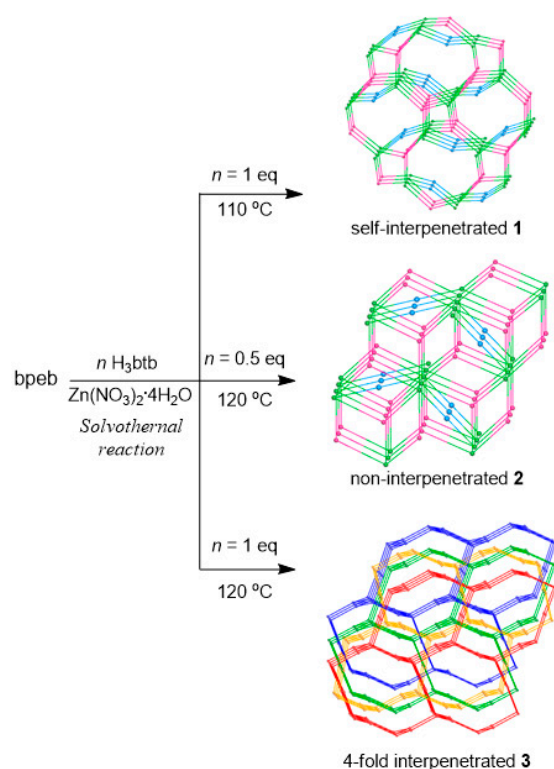


**Figure 2.** The details of synthetic procedures of 1–3.

#### 3.2. Structural Description of $[\text{Zn}_2(\text{bpeb})(\text{btb})(\text{OH})] \cdot \text{DMF} \cdot \text{H}_2\text{O}$ (1)

The green block-shaped single crystals of  $[\text{Zn}_2(\text{bpeb})(\text{btb})(\text{OH})] \cdot \text{DMF} \cdot \text{H}_2\text{O}$  (1) were synthesized through a solvothermal reaction. This reaction involved combining zinc(II) salt, bpeb, and  $\text{H}_3\text{btb}$  in an equimolar stoichiometry using a mixture of dimethylformamide (DMF),  $\text{H}_2\text{O}$ , and dimethylsulfoxide (DMSO) at 110 °C (as shown in Figure 3). The single-crystal X-ray diffraction (SC-XRD) analysis revealed that 1 crystallized in orthorhombic *Fdd2* with  $Z = 8$ . Within the asymmetric unit, there exist two zinc(II) atoms, one btb, one bpeb, and one hydroxide ion (Figure 3). The Zn1 and Zn2 atoms in the repeating unit show different coordination geometries. The Zn1 has a distorted square pyramidal geometry with O3 and O4 from a chelating carboxylate ion, O1 from one bridging carboxylate of btb ligands, and one N atom of the bpeb ligand in the square plane. Further, the oxygen atom of the hydroxide ion is in the apical position. In Zn2, the coordination environment is shown as having a distorted trigonal bipyramidal geometry with O6 from a chelating carboxylate and O1s from a hydroxide ion, a nitrogen atom (N2) defining the trigonal plane, and the axial positions occupied by O2 and O5 oxygen atoms from two different btb ligands. The bpeb ligand has a *trans-cis-trans* conformation, as shown in Figure 3b.

In the literature, when carboxylate was changed from btb to biphenyl-4,4'-dicarboxylate (bpdC), triply interpenetrated 3D MOF  $[\text{Zn}_3(\text{bpdC})_3(\text{bpeb})] \cdot 0.5\text{DMSO} \cdot 1.5\text{H}_2\text{O}$  showing the same molecular building block  $[\text{Zn}_3(\text{O}_2\text{C-R})_6(\text{py})_2]$  as Zn1-Zn2-Zn1A with a perfect linear angle of  $180.0^\circ$  was obtained [49]. However, in the case of MOF **1**, Zn1-Zn2-Zn1A was bent with an angle of  $153.1^\circ$ . The tilting of the molecular building blocks is predicted to be caused by the btb tricarboxylate as a large molecule. In the large void generated by the angular tricarboxylate ( $120^\circ$ ), btb was filled via self-interpenetration. The calculated total potential solvent area volume in compound **1**, as determined by PLATON [48], amounts to  $8723.8 \text{ \AA}^3$ , which corresponds to 39.1% of the unit cell volume ( $22,321.4 \text{ \AA}^3$ ), even in the presence of self-interpenetration. Notably, the solvent's unoccupied space was effectively filled by well-ordered DMF and water molecules.

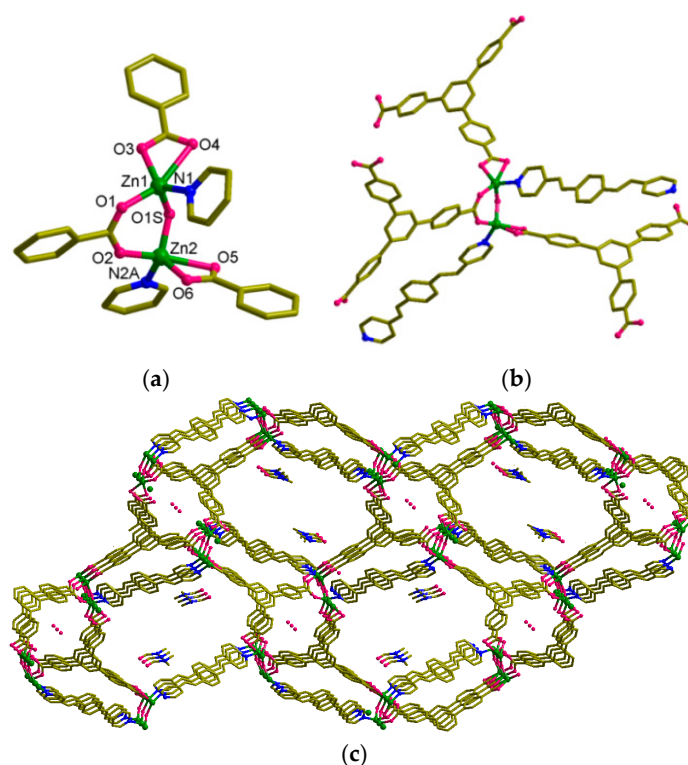


**Figure 3.** Crystal structure of  $[\text{Zn}_2(\text{bpeb})(\text{btb})(\text{OH})] \cdot \text{DMF} \cdot \text{H}_2\text{O}$  (**1**): (a) Coordination environments of Zn1 and Zn2. (b) A general view around zinc(II) in **1**. (c) A self-interpenetration, with channels along the *c*-axis in **1**.

### 3.3. Structural Description of $[\text{Zn}_3(\text{btb})_2(\text{bpeb})] \cdot x\text{Solvent}$ (**2**)

The green plate-shaped single crystals of  $[\text{Zn}_3(\text{btb})_2(\text{bpeb})] \cdot x\text{Solvent}$  (**2**) were synthesized through a solvothermal reaction. This reaction involved combining zinc(II) salt, bpeb, and  $\text{H}_3\text{btb}$  in a 1:1:0.5 molar ratio stoichiometry using a mixture of DMF,  $\text{H}_2\text{O}$ , and DMSO at  $110^\circ\text{C}$  (as shown in Figure 4). The SC-XRD analysis revealed that **2** crystallizes in monoclinic  $\text{C}2/c$  with  $Z = 4$ . The asymmetric unit contains one and a half zinc(II) atoms, one btb, and half of a bpeb ligand (as shown in Figure 4). The crystallographic twofold axis at Zn2 generates the whole repeating unit. In the case of the molecular building unit  $[\text{Zn}_3\text{btb}_2]$ , the arrangement of the three zinc(II) atoms is linear, and this configuration is bridged by three carboxylate ligands connecting each pair of Zn2 atoms. As a result, the central Zn2 atom adopts a distorted octahedral geometry, forming a  $\text{ZnO}_6$  core, as visually depicted in Figure 4a. In the context of this depiction, each of the “terminal” Zn1 atoms within the linear trinuclear complex exhibits a tetrahedral geometry. These Zn1 atoms are bonded to three oxygen atoms, specifically O1, O4, and O5, originating from three distinct btb ligands. A relatively weaker interaction between Zn1 and O3 ( $2.64 \text{ \AA}$ ) is

observed. The Zn<sub>3</sub> rod consists of two pyramidal-shaped ZnO<sub>3</sub> cores that are staggered but positioned in a face-to-face orientation, as illustrated in Figure 4a. In the repeating unit [Zn<sub>3</sub>(O<sub>2</sub>C-R)<sub>6</sub>(py)<sub>2</sub>], each Zn1 atom's tetrahedral geometry is fulfilled through the inclusion of a N atom from the bpeb ligand. Recently, this repeating unit was reported by us. The single-stranded helix consists of the [Zn<sub>3</sub>(btb)<sub>3</sub>] unit from the double interpenetration (Figure 4d). The bpeb penetrates the [Zn<sub>3</sub>(btb)<sub>2</sub>] square unit to form a rotaxane structure (Figure 4e). To our knowledge, this represents a unique example of a coordination-based polyrotaxane. Recently, 2D polyrotaxane-type coordination polymers were reported by us [50–54]. The empty space volume as calculated by PLATON [48] in **2**, 4496.8 Å<sup>3</sup>, is 47.4% of the unit cell volume, 9490.1 Å<sup>3</sup>. The void volume was filled by solvent molecules in a disordered arrangement.

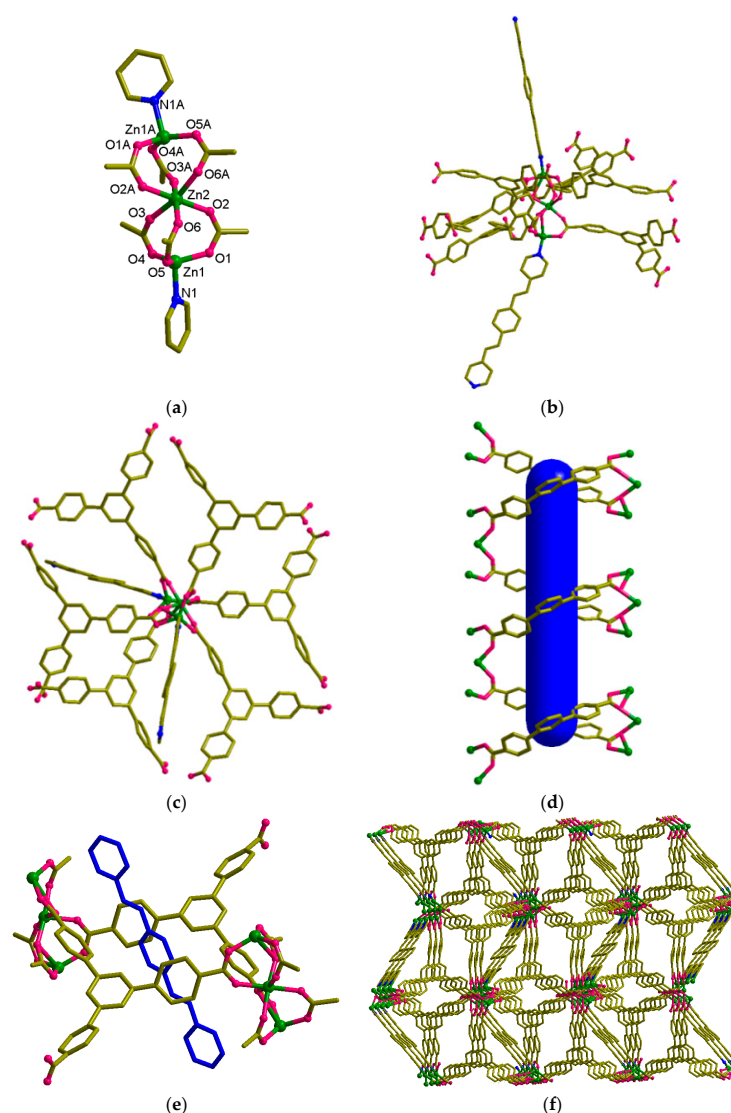


**Figure 4.** Noninterpenetrated structure of **2**: (a) Atom labeling in the SBU core. Symmetry operator  $A = x, y - 1, z$ . (b) A general view incorporating zinc(II) ion. (c) A top view of SBU. (d) Helix type of the [Zn<sub>3</sub>(btb)<sub>2</sub>] unit. (e) Rotaxane unit. (f) A portion of the 3D network structure showing the channels along the *a*-axis.

### 3.4. Structural Description of [Zn<sub>2</sub>(Hbtb)<sub>2</sub>(bpeb)][Zn<sub>2</sub>(Hbtb)<sub>2</sub>(bpeb)][Zn<sub>4</sub>(Hbtb)<sub>4</sub>(bpeb)<sub>2</sub>] $\cdot$ *x*Solvent (**3**)

The green plate-shaped single crystals of [Zn<sub>2</sub>(Hbtb)<sub>2</sub>(bpeb)][Zn<sub>2</sub>(Hbtb)<sub>2</sub>(bpeb)][Zn<sub>4</sub>(Hbtb)<sub>4</sub>(bpeb)<sub>2</sub>] $\cdot$ *x*Solvent (**3**) were isolated via a solvothermal reaction of zinc(II) salt, H<sub>3</sub>btb, and bpeb in an equimolar ratio from a mixture of DMF, DMSO, and water at 120 °C (Table 1).

The SC-XRD analysis revealed that **3** crystallized in monoclinic  $P2_1/c$  with  $Z = 2$ . Unusually, the asymmetric unit in **3** contains three parts. The first part includes Zn1 (Figure 5a,d, red part): one Zn(II) atom, one Hbtb, and one-half bpeb. And the second part involves Zn2 (Figure 5b,d, blue part): one zinc(II) atom, one Hbtb, and one-half bpeb. The third part contains Zn3 and Zn4 (Figure 5c,d, green part): two Zn(II) atoms, two Hbtb, and one bpeb. All of the zinc(II) atoms show tetrahedral coordination geometry. For example, the Zn1 with a distorted tetrahedral geometry is coordinated to one *N* atom of the bpeb spacer ligands and three *O* atoms of the btb ligands (Figure 5a). The distances of  $Zn1 \cdots O2$ ,  $Zn1 \cdots O3A$ , and  $Zn1 \cdots O6B$  are 3.0311(2), 3.0786(2), and 2.8154(1) Å, respectively, indicating that the carbonyl oxygen atoms are nonbonded. In the four-fold interpenetrated structure shown in Figure 5e, each of the red, blue, or green and light green single frameworks originates from the red, blue, or green asymmetric units shown in Figure 5d, respectively. The calculated total potential solvent area volume in compound **2**, as determined by PLATON [48], amounts to 11,462.1 Å<sup>3</sup>, which corresponds to 53.7% of the unit cell volume (21,346.0 Å<sup>3</sup>), even in the presence of four-fold interpenetration. Notably, the solvent's unoccupied space was effectively filled by disordered DMF and water molecules.

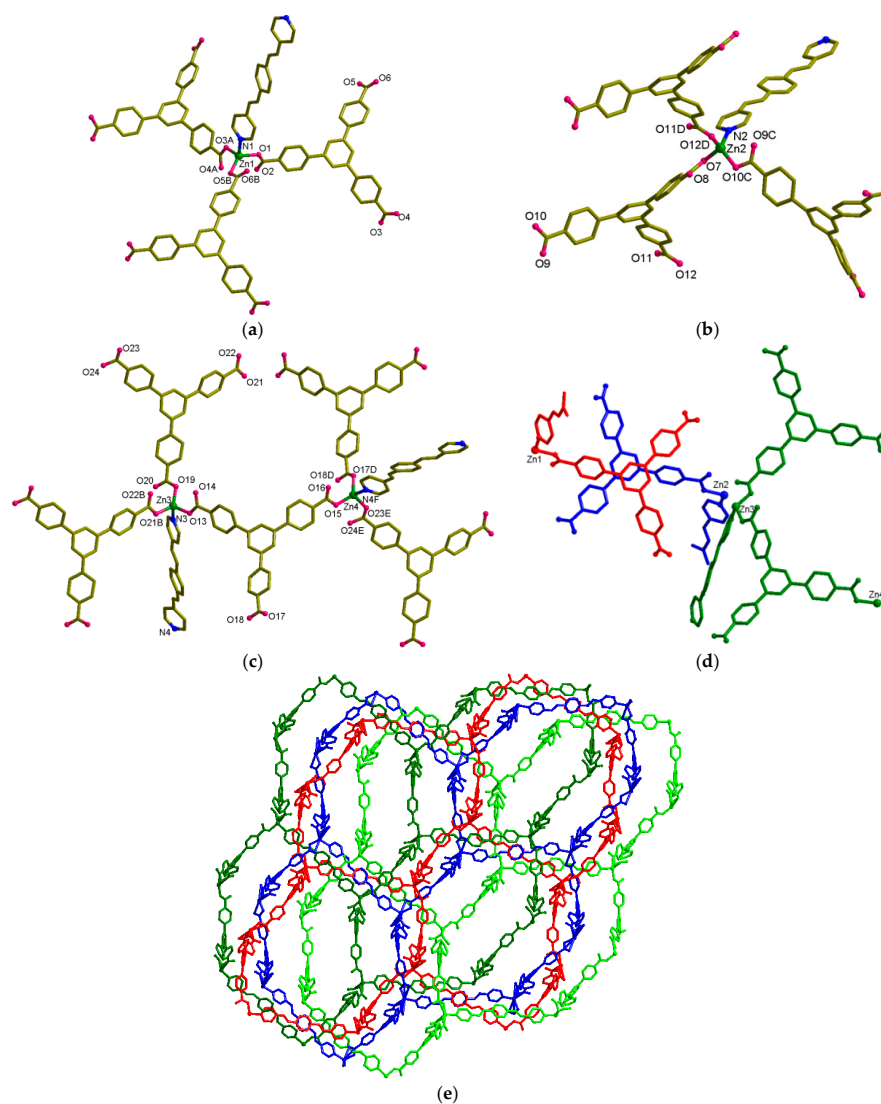


**Figure 5.** Four-interpenetrated 3D structure of **3**: A general view incorporating (a) Zn1, (b) Zn2, and (c) Zn3 and Zn4. (d) Asymmetric unit. (e) A four-interpenetration, with channels along the *a*-axis.

### 3.5. Thermal Stability

Thermal gravimetric analysis (TGA) experiments were carried out to investigate the thermal stability of MOFs 1–3, as depicted in Figures S5–S7. The samples underwent a gradual temperature increase at a constant rate of 10 °C per minute, commencing from room temperature and heating up to 700 °C, all in an uninterrupted stream of N<sub>2</sub> gas. The analysis of the TGA data revealed that MOFs 1–3 exhibited thermal stability up to temperatures ranging from 360 to 380 °C. Furthermore, it was verified that the solvents within the structure of all MOFs displayed values consistent with the findings from elemental analysis. The lattice solvents in 1 and 3 were notably eliminated post 220 °C. However, the solvent molecules in 2 were progressively removed until approximately 270 °C.

### 3.6. Topological Analysis

The topologies of MOFs 1–3 were analyzed using the ToposPro program [55–57]. The centers of zinc(II) atoms and btb ligands were considered to be connected nodes. MOFs 1–3 show all the new topologies. In the context of MOFs, a new topology refers to a novel arrangement of the metal nodes and organic compounds that form the underlying framework structure of the MOF. The reason for new topologies in MOFs 1–3 could be attributed to the long spacer, bpeb, and tricarboxylate coligand as a large molecule incorporating three directions.

By considering the center of the bpeb ligand, the Zn cation, and the btb ligand in 1 as 2-, 3-, and 5-connected nodes, respectively, the overall topology belongs to a (2,3,5)-connected point symbol  $\{8.10^2\}\{8^4.10^5.12\}\{8\}$  net, which is a new topology. In 2, the incorporation of the bpeb node, the Zn node, and the btb ligand node as 2-, 3-, and 8-connected nodes, respectively, results in the overall topology being categorized as a new topology with a (2,3,8)-connected point symbol  $\{4^2.6\}2\{4^4.6^2.8^{20}.10.12\}\{8\}$  net. In the case of 3, considering the bpeb node, the Zn node, and the btb node as having connectivities of 2, 3, and 4, respectively, the resultant topology can be identified as a new topology, a (2,3,4)-connected point symbol  $\{6^3.8^2.10\}2\{6^3\}2\{8\}$  net.

### 3.7. Solid-State Emission

The luminescence properties of these MOFs (1–3) in the solid state were investigated as *d*<sup>10</sup> Zn(II) carboxylates exhibited this photoluminescence property, and the results are shown in Figure 6 [58–60]. MOF 1 shows a strong blue emission with the peak centered at 448 nm. MOF 2 also exhibits a strong blue emission centered at 452 nm with a slightly shifted peak similar to MOF 1. However, while MOF 1 and MOF 2 emit light that appears similar, MOF 3 exhibits a comparatively weaker greenish emission, with the peak centered around 494 nm. It is interesting that despite having identical metal cations, anions, and spacer ligands, the three MOFs exhibit distinct different emissions as a result of their differing structures and connectivities [61]. This implies that the variations in their structures and connectivities result in distinct luminescent properties. The differences in the arrangement of the metal cations and organic compounds within the framework can lead to different energy states for the luminescent centers or varying degrees of interaction between them. As a consequence, the emission spectrum, intensity, and efficiency of the MOFs will differ.

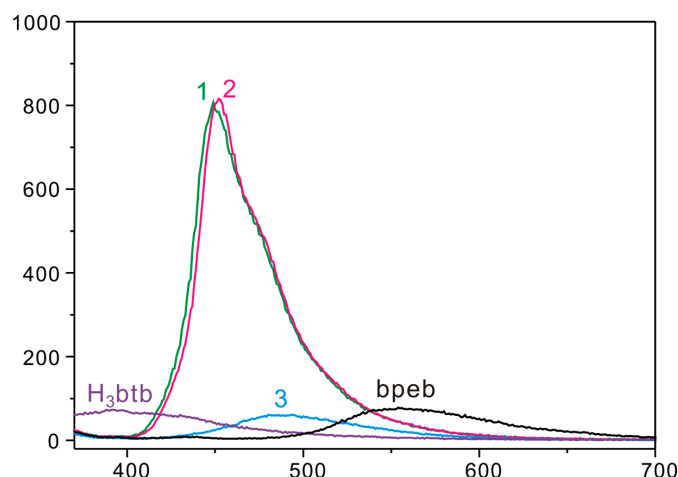


**Figure 6.** Emission spectra of MOFs 1–3 in the solid state at room temperature (excited at 360 nm).

#### 4. Conclusions

To summarize, three-dimensional Zn(II) metal-organic frameworks (MOFs) with dipyriddylolefin as a long spacer and tricarboxylate ligands were successfully synthesized and characterized. Solvothermal reactions led to the formation of three distinct Zn(II) MOFs (1–3), which exhibited different structures and interpenetration motifs depending on the temperature and mole-ratio variations. Despite having identical metal cations, anions, and spacer ligands, these MOFs displayed diverse emission properties, highlighting the significant impact of their unique structures and connectivities on their luminescent behavior. These findings underscore the importance of structural design in tailoring the properties of MOFs for potential applications in various fields.

**Supplementary Materials:** The following supporting information can be downloaded at <https://www.mdpi.com/article/10.3390/cryst13081266/s1>, Experimental Section; Figure S1. Crystal structure of 2 showing whole btb molecules disordered in two positions (blue: yellow = 53:47); Figure S2. PXRD patterns for 1: (top) as-synthesized and (bottom) simulated from the single-crystal X-ray data; Figure S3. PXRD patterns for 2: (top) as-synthesized and (bottom) simulated from the single-crystal X-ray data; Figure S4. PXRD patterns for 3: (top) as-synthesized and (bottom) simulated from the single-crystal X-ray data; Figure S5. TGA curve of 1; Figure S6. TGA curve of 2; Figure S7. TGA curve of 3; Figure S8. Topological representation of 1; Figure S9. Topological representation of 2; Figure S10. Topological representation of 3 showing (a) a single network and (b) four-fold interpenetration. Refs. [62–64] cited in Supplementary Materials.

**Author Contributions:** Conceptualization, I.-H.P.; methodology, I.-H.P.; validation, D.H.L.; formal analysis, D.H.L. and I.-H.P.; investigation, D.H.L. and I.-H.P.; resources, I.-H.P.; data curation, D.H.L. and I.-H.P.; writing—original draft preparation, D.H.L. and I.-H.P.; writing—review and editing, D.H.L. and I.-H.P.; visualization, I.-H.P.; supervision, I.-H.P.; project administration, I.-H.P.; funding acquisition, I.-H.P. All authors have read and agreed to the published version of the manuscript.

**Funding:** This work was supported by the research fund of Chungnam National University.

**Data Availability Statement:** The data presented in this study are available in the Supplementary Materials.

**Acknowledgments:** All authors sincerely acknowledge Shim Sung Lee and Jagadese J. Vittal for their critical comments and interest in this project. We thank Eunji Lee for her help in topological analysis and fruitful discussions.

**Conflicts of Interest:** The authors declare no conflict of interest.

**Sample Availability:** Samples of the compounds are not available from the authors.

## References

1. Morris, R.E.; Brammer, L. Coordination change, lability and hemilability in metal–organic frameworks. *Chem. Soc. Rev.* **2017**, *46*, 5444–5462. [[CrossRef](#)] [[PubMed](#)]
2. Kole, G.K.; Vittal, J.J. Solid-state reactivity and structural transformations involving coordination polymers. *Chem. Soc. Rev.* **2013**, *42*, 1755–1775. [[CrossRef](#)]
3. Desiraju, G.R. Crystal Engineering: From Molecule to Crystal. *J. Am. Chem. Soc.* **2013**, *135*, 9952–9967. [[CrossRef](#)] [[PubMed](#)]
4. Moulton, B.; Zaworotko, M.J. From Molecules to Crystal Engineering: Supramolecular Isomerism and Polymorphism in Network Solids. *Chem. Rev.* **2001**, *101*, 1629–1658. [[CrossRef](#)] [[PubMed](#)]
5. Cohen, S.M. Modifying MOFs: New chemistry, new materials. *Chem. Sci.* **2010**, *1*, 32–36. [[CrossRef](#)]
6. Wang, Z.; Cohen, S.M. Postsynthetic modification of metal–organic frameworks. *Chem. Soc. Rev.* **2009**, *38*, 1315–1329. [[CrossRef](#)]
7. Chakraborty, G.; Park, I.-H.; Medishetty, R.; Vittal, J.J. Two-Dimensional Metal–Organic Framework Materials: Synthesis, Structures, Properties and Applications. *Chem. Rev.* **2021**, *121*, 3751–3891. [[CrossRef](#)]
8. Zhou, H.-C.; Long, J.R.; Yaghi, O.M. Introduction to Metal–Organic Frameworks. *Chem. Rev.* **2012**, *112*, 673–674. [[CrossRef](#)]
9. Houck, H.A.; Du Prez, F.E.; Barner-Kowollik, C. Controlling thermal reactivity with different colors of light. *Nat. Commun.* **2017**, *8*, 1869. [[CrossRef](#)]
10. Kitagawa, S.; Kitaura, R.; Noro, S.I. Functional Porous Coordination Polymers. *Angew. Chem. Int. Ed.* **2004**, *43*, 2334–2375. [[CrossRef](#)]
11. Park, I.-H.; Mulijanto, C.E.; Lee, H.-H.; Kang, Y.; Lee, E.; Chanthapally, A.; Lee, S.S.; Vittal, J.J. Influence of Interpenetration in Diamondoid Metal–Organic Frameworks on the Photoreactivity and Sensing Properties. *Cryst. Growth Des.* **2016**, *16*, 2504–2508. [[CrossRef](#)]
12. Eddaoudi, M.; Kim, J.; Rosi, N.; Vodak, D.; Wachter, J.; Keeffe, M.; Yaghi, O.M. Systematic Design of Pore Size and Functionality in Isoreticular MOFs and Their Application in Methane Storage. *Science* **2002**, *295*, 469. [[CrossRef](#)]
13. Horike, S.; Shimomura, S.; Kitagawa, S. Soft porous crystals. *Nat. Chem.* **2009**, *1*, 695–704. [[CrossRef](#)]
14. Farha, O.K.; Hupp, J.T. Rational Design, Synthesis, Purification, and Activation of Metal–Organic Framework Materials. *Acc. Chem. Res.* **2010**, *43*, 1166–1175. [[CrossRef](#)] [[PubMed](#)]
15. Zhang, J.; Wojtas, L.; Larsen, R.W.; Eddaoudi, M.; Zaworotko, M.J. Temperature and Concentration Control over Interpenetration in a Metal–Organic Material. *J. Am. Chem. Soc.* **2009**, *131*, 17040–17041. [[CrossRef](#)] [[PubMed](#)]
16. Klein, N.; Senkovska, I.; Gedrich, K.; Stoeck, U.; Henschel, A.; Mueller, U.; Kaskel, S. A Mesoporous Metal–Organic Framework. *Angew. Chem. Int. Ed.* **2009**, *48*, 9954–9957. [[CrossRef](#)]
17. Férey, G. Hybrid porous solids: Past, present, future. *Chem. Soc. Rev.* **2008**, *37*, 191–214. [[CrossRef](#)]
18. Batten, S.R.; Robson, R. Interpenetrating Nets: Ordered, Periodic Entanglement. *Angew. Chem. Int. Ed.* **1998**, *37*, 1460–1494. [[CrossRef](#)]
19. Gupta, M.; Vittal, J.J. Control of interpenetration and structural transformations in the interpenetrated MOFs. *Coord. Chem. Rev.* **2021**, *435*, 213789. [[CrossRef](#)]
20. Chen, Z.; Gallo, G.; Sawant, V.A.; Zhang, T.; Zhu, M.; Liang, L.; Chanthapally, A.; Bolla, G.; Quah, H.S.; Liu, X.; et al. Giant Enhancement of Second Harmonic Generation Accompanied by the Structural Transformation of 7-Fold to 8-Fold Interpenetrated Metal–Organic Frameworks (MOFs). *Angew. Chem. Int. Ed.* **2020**, *59*, 833–838. [[CrossRef](#)]
21. Elsaidi, S.K.; Mohamed, M.H.; Wojtas, L.; Chanthapally, A.; Pham, T.; Space, B.; Vittal, J.J.; Zaworotko, M.J. Putting the Squeeze on CH<sub>4</sub> and CO<sub>2</sub> through Control over Interpenetration in Diamondoid Nets. *J. Am. Chem. Soc.* **2014**, *136*, 5072–5077. [[CrossRef](#)]
22. Yang, G.-P.; Hou, L.; Luan, X.-J.; Wu, B.; Wang, Y.-Y. Molecular braids in metal–organic frameworks. *Chem. Soc. Rev.* **2012**, *41*, 6992–7000. [[CrossRef](#)]
23. Jiang, H.-L.; Makal, T.A.; Zhou, H.-C. Interpenetration control in metal–organic frameworks for functional applications. *Coord. Chem. Rev.* **2013**, *257*, 2232–2249. [[CrossRef](#)]
24. Dezotti, Y.; Ribeiro, M.A.; Pirota, K.R.; Barros, W.P. Influence of the Metal Ion on the Topology and Interpenetration of Pyridylvinyl(benzoate) Based Metal–Organic Frameworks. *Cryst. Growth Des.* **2019**, *19*, 5592–5603. [[CrossRef](#)]
25. Bae, C.; Gu, M.; Jeon, Y.; Kim, D.; Kim, J. Metal–organic frameworks for NH<sub>3</sub> adsorption by different NH<sub>3</sub> operating pressures. *Bull. Korean Chem. Soc.* **2023**, *44*, 112–124. [[CrossRef](#)]
26. Choi, I.-H.; Gu, J.-M.; Kim, H.-C.; Kim, Y.; Huh, S. Gas sorption properties of a new Zn-BTB metal–organic framework with permanent porosity. *Bull. Korean Chem. Soc.* **2023**. *Early view*. [[CrossRef](#)]
27. Jeong, J.Y.; Joung, H.; Jang, G.J.; Han, S.Y. Probing emergence of biomolecular coronas around drug-loaded liposomal nanoparticles in the solution by using nanoparticle tracking analysis. *Bull. Korean Chem. Soc.* **2023**, *44*, 551–557. [[CrossRef](#)]
28. Kim, J.; Na, C.; Son, Y.; Prabu, M.; Yoon, M. Stilbene ligand-based metal–organic frameworks for efficient dye adsorption and nitrobenzene detection. *Bull. Korean Chem. Soc.* **2023**, *44*, 507–515. [[CrossRef](#)]
29. Lee, D.; Lee, S.; Son, Y.; Kim, J.Y.; Cha, S.; Kwak, D.; Lee, J.; Kwak, J.; Yoon, M.; Kim, M. Uncoordinated tetrazole ligands in metal–organic frameworks for proton-conductivity studies. *Bull. Korean Chem. Soc.* **2022**, *43*, 912–917. [[CrossRef](#)]
30. Park, J.H.; Lee, W.R.; Kim, Y.; Lee, H.J.; Ryu, D.W.; Phang, W.J.; Hong, C.S. Interpenetration Control, Sorption Behavior, and Framework Flexibility in Zn(II) Metal–Organic Frameworks. *Cryst. Growth Des.* **2014**, *14*, 699–704. [[CrossRef](#)]
31. Shekhah, O.; Wang, H.; Paradinas, M.; Ocal, C.; Schüpbach, B.; Terfort, A.; Zacher, D.; Fischer, R.A.; Wöll, C. Controlling interpenetration in metal–organic frameworks by liquid-phase epitaxy. *Nat. Mater.* **2009**, *8*, 481–484. [[CrossRef](#)] [[PubMed](#)]

32. Kim, J.; Yang, S.-T.; Choi, S.B.; Sim, J.; Kim, J.; Ahn, W.-S. Control of catenation in CuTATB-n metal–organic frameworks by sonochemical synthesis and its effect on CO<sub>2</sub> adsorption. *J. Mater. Chem.* **2011**, *21*, 3070–3076. [[CrossRef](#)]
33. Evans, O.R.; Lin, W. Rational Design of Nonlinear Optical Materials Based on 2D Coordination Networks. *Chem. Mater.* **2001**, *13*, 3009–3017. [[CrossRef](#)]
34. Ma, L.; Lin, W. Chirality-Controlled and Solvent-Templated Catenation Isomerism in Metal–Organic Frameworks. *J. Am. Chem. Soc.* **2008**, *130*, 13834–13835. [[CrossRef](#)] [[PubMed](#)]
35. Guo, M.; Sun, Z.-M. Solvents control over the degree of interpenetration in metal-organic frameworks and their high sensitivities for detecting nitrobenzene at ppm level. *J. Mater. Chem.* **2012**, *22*, 15939–15946. [[CrossRef](#)]
36. Evans, O.R.; Lin, W. Crystal Engineering of Nonlinear Optical Materials Based on Interpenetrated Diamondoid Coordination Networks. *Chem. Mater.* **2001**, *13*, 2705–2712. [[CrossRef](#)]
37. Song, F.; Wang, C.; Falkowski, J.M.; Ma, L.; Lin, W. Isoreticular Chiral Metal–Organic Frameworks for Asymmetric Alkene Epoxidation: Tuning Catalytic Activity by Controlling Framework Catenation and Varying Open Channel Sizes. *J. Am. Chem. Soc.* **2010**, *132*, 15390–15398. [[CrossRef](#)]
38. Evans, O.R.; Lin, W. Crystal Engineering of NLO Materials Based on Metal–Organic Coordination Networks. *Acc. Chem. Res.* **2002**, *35*, 511–522. [[CrossRef](#)]
39. Katz, M.J.; Rannal, T.; Yu, H.-Z.; Leznoff, D.B. Polymorphism of Zn[Au(CN)<sub>2</sub>]<sub>2</sub> and Its Luminescent Sensory Response to NH<sub>3</sub> Vapor. *J. Am. Chem. Soc.* **2008**, *130*, 10662–10673. [[CrossRef](#)]
40. Liu, D.; Li, H.-X.; Liu, L.-L.; Wang, H.-M.; Li, N.-Y.; Ren, Z.-G.; Lang, J.-P. How do substituent groups in the 5-position of 1,3-benzenedicarboxylate affect the construction of supramolecular frameworks? *CrystEngComm* **2010**, *12*, 3708–3716. [[CrossRef](#)]
41. Li, F.F.; Zhang, L.; Gong, L.L.; Yan, C.S.; Gao, H.Y.; Luo, F. Reversible photo/thermoswitchable dual-color fluorescence through single-crystal-to-single-crystal transformation. *Dalton Trans.* **2017**, *46*, 338–341. [[CrossRef](#)] [[PubMed](#)]
42. Quah, H.S.; Nalla, V.; Zheng, K.; Lee, C.A.; Liu, X.; Vittal, J.J. Tuning Two-Photon Absorption Cross Section in Metal Organic Frameworks. *Chem. Mater.* **2017**, *29*, 7424–7430. [[CrossRef](#)]
43. Park, I.-H.; Ju, H.; Kim, K.; Lee, S.S.; Vittal, J.J. Isomerism in double-pillared-layer coordination polymers—Structures and photoreactivity. *IUCr* **2018**, *5*, 182–189. [[CrossRef](#)] [[PubMed](#)]
44. Gutov, A.V.; Rusanov, E.B.; Chepeleva, L.V.; Garasevich, S.G.; Ryabitskii, A.B.; Chernega, A.N. New viologen analogs: 1,4-bis[2-(pyridin-4-yl)ethenyl]benzene quaternary salts. *Russ. J. Gen. Chem.* **2009**, *79*, 1513–1518. [[CrossRef](#)]
45. Bruker, A.J.B.A.I. *Saint and SADABS*; Bruker AXS Inc.: Madison, WI, USA, 2009.
46. Sheldrick, G.M. *SADABS*, Version 2.03; University of Göttingen: Göttingen, Germany, 2002.
47. Bruker, A.I.; Madison, W. *SHELXTL*, Version 6.10; Bruker AXS Inc.: Madison, WI, USA, 2000.
48. Spek, A. PLATON SQUEEZE: A tool for the calculation of the disordered solvent contribution to the calculated structure factors. *Acta Crystallogr. C* **2015**, *71*, 9–18. [[CrossRef](#)]
49. Park, I.-H.; Kim, K.; Lee, S.S.; Vittal, J.J. An Unusual Interweaving in a 3-Fold Interpenetrated Pillared-Layer Zn(II) Coordination Polymer with a Long Spacer Ligand. *Cryst. Growth Des.* **2012**, *12*, 3397–3401. [[CrossRef](#)]
50. Park, I.-H.; Medishetty, R.; Kim, J.-Y.; Lee, S.S.; Vittal, J.J. Distortional Supramolecular Isomers of Polyrotaxane Coordination Polymers: Photoreactivity and Sensing of Nitro Compounds. *Angew. Chem. Int. Ed.* **2014**, *53*, 5591–5595. [[CrossRef](#)]
51. Park, I.-H.; Medishetty, R.; Lee, S.S.; Vittal, J.J. Solid-state polymerization in a polyrotaxane coordination polymer via a [2 + 2] cycloaddition reaction. *Chem. Commun.* **2014**, *50*, 6585–6588. [[CrossRef](#)]
52. Park, I.-H.; Heng, T.S.; Ju, H.; Ding, J.; Lee, S.S.; Vittal, J.J. Synthesis, structures and magnetic properties of isoreticular polyrotaxane-type two-dimensional coordination polymers. *RSC Adv.* **2017**, *7*, 45582–45586. [[CrossRef](#)]
53. Park, I.-H.; Ju, H.; Heng, T.S.; Kang, Y.; Lee, S.S.; Ding, J.; Vittal, J.J. Supramolecular Isomerism and Polyrotaxane-Based Two-Dimensional Coordination Polymers. *Cryst. Growth Des.* **2016**, *16*, 7278–7285. [[CrossRef](#)]
54. Ju, H.; Shin, M.; Park, I.-H.; Jung, J.H.; Vittal, J.J.; Lee, S.S. Construction of 2D Interdigitated Polyrotaxane Layers and their Transformation to a 3D Polyrotaxane by a Photocycloaddition Reaction between Wheels. *Inorg. Chem.* **2021**, *60*, 8285–8292. [[CrossRef](#)]
55. Blatov, V.A. Nanocluster analysis of intermetallic structures with the program package TOPOS. *Struct. Chem.* **2012**, *23*, 955–963. [[CrossRef](#)]
56. Alexandrov, E.V.; Blatov, V.A.; Kochetkov, A.V.; Proserpio, D.M. Underlying nets in three-periodic coordination polymers: Topology, taxonomy and prediction from a computer-aided analysis of the Cambridge Structural Database. *CrystEngComm* **2011**, *13*, 3947–3958. [[CrossRef](#)]
57. Blatov, V.A.; Shevchenko, A.P.; Proserpio, D.M. Applied Topological Analysis of Crystal Structures with the Program Package ToposPro. *Cryst. Growth Des.* **2014**, *14*, 3576–3586. [[CrossRef](#)]
58. Yam, V.W.-W.; Au, V.K.-M.; Leung, S.Y.-L. Light-Emitting Self-Assembled Materials Based on d<sup>8</sup> and d<sup>10</sup> Transition Metal Complexes. *Chem. Rev.* **2015**, *115*, 7589–7728. [[CrossRef](#)]
59. Li, S.-L.; Lan, Y.-Q.; Ma, J.-F.; Fu, Y.-M.; Yang, J.; Ping, G.-J.; Liu, J.; Su, Z.-M. Structures and Luminescent Properties of a Series of Zinc(II) and Cadmium(II) 4,4'-Oxydiphthalate Coordination Polymers with Various Ligands Based on Bis(pyridyl imidazole) under Hydrothermal Conditions. *Cryst. Growth Des.* **2008**, *8*, 1610–1616. [[CrossRef](#)]

60. Guo, H.-D.; Guo, X.-M.; Batten, S.R.; Song, J.-F.; Song, S.-Y.; Dang, S.; Zheng, G.-L.; Tang, J.-K.; Zhang, H.-J. Hydrothermal Synthesis, Structures, and Luminescent Properties of Seven d10 Metal–Organic Frameworks Based on 9,9-Dipropylfluorene-2,7-Dicarboxylic Acid (H<sub>2</sub>DFDA). *Cryst. Growth Des.* **2009**, *9*, 1394–1401. [[CrossRef](#)]
61. Bauer, C.A.; Timofeeva, T.V.; Settersten, T.B.; Patterson, B.D.; Liu, V.H.; Simmons, B.A.; Allendorf, M.D. Influence of Connectivity and Porosity on Ligand-Based Luminescence in Zinc Metal–Organic Frameworks. *J. Am. Chem. Soc.* **2007**, *129*, 7136–7144. [[CrossRef](#)]
62. Duan, J.; Higuchi, M.; Foo, M.L.; Horike, S.; Rao, K.P.; Kitagawa, S. A Family of Rare Earth Porous Coordination Polymers with Different Flexibility for CO<sub>2</sub>/C<sub>2</sub>H<sub>4</sub> and CO<sub>2</sub>/C<sub>2</sub>H<sub>6</sub> Separation. *Inorg. Chem.* **2013**, *52*, 8244–8249. [[CrossRef](#)]
63. Henke, S.; Schmid, R.; Grunwaldt, J.-D.; Fischer, R.A. Flexibility and Sorption Selectivity in Rigid Metal–Organic Frameworks: The Impact of Ether-Functionalised Linkers. *Chem. Eur. J.* **2010**, *16*, 14296–14306. [[CrossRef](#)]
64. Kaneko, W.; Ohba, M.; Kitagawa, S. A Flexible Coordination Polymer Crystal Providing Reversible Structural and Magnetic Conversions. *J. Am. Chem. Soc.* **2007**, *129*, 13706–13712. [[CrossRef](#)]

**Disclaimer/Publisher’s Note:** The statements, opinions and data contained in all publications are solely those of the individual author(s) and contributor(s) and not of MDPI and/or the editor(s). MDPI and/or the editor(s) disclaim responsibility for any injury to people or property resulting from any ideas, methods, instructions or products referred to in the content.